separations

MDPI

Article

Facile Separation of Cu^{2+} from Water by Novel Sandwich NaY Zeolite Adsorptive Membrane

Yuexin Guo [1,*,†], Xu Zhang [1,†], Yuesheng Xie [1], Yacong Hu [1], Zhiqian Jia [2,*], Yafei Ma [1] and Xin Wang [1]

[1] School of Pharmacy, North China University of Science and Technology, Tangshan 063210, China
[2] College of Chemistry, Beijing Normal University, Beijing 100875, China
* Correspondence: yuexinguo@126.com (Y.G.); zhqjia@bnu.edu.cn (Z.J.)
† These authors contributed equally to this work.

Abstract: Polyethersulfone-sulfonated polyethersulfone (PES-SPES)/NaY zeolite/nylon sandwich structure membranes were prepared and used to adsorb Cu^{2+} from water. The adsorption kinetics, adsorption isotherm, dynamic adsorption experiment, and reusability were discussed. The experimental data showed that the Langmuir isotherm model, Dubinin–Radushkevich (D-R) isotherm model, and the pseudo-first-order kinetic model can well represent the adsorption of Cu^{2+} on the membrane, indicating an ion exchange mechanism, with the maximum adsorption capacity of 111.25 $mg \cdot g^{-1}$. Repeatability experiments show that the sandwich film still has good adsorption performance after five times of adsorption and desorption. The as-prepared membrane showed considerable separation performance in removing Cu^{2+} from aspirin solution, providing a feasible method to remove heavy metals from drugs.

Keywords: adsorptive membrane; sandwich structure; NaY zeolite; Cu^{2+}

Citation: Guo, Y.; Zhang, X.; Xie, Y.; Hu, Y.; Jia, Z.; Ma, Y.; Wang, X. Facile Separation of Cu^{2+} from Water by Novel Sandwich NaY Zeolite Adsorptive Membrane. *Separations* **2023**, *10*, 171. https://doi.org/10.3390/separations10030171

Academic Editor: Mingheng Li

Received: 30 January 2023
Revised: 27 February 2023
Accepted: 28 February 2023
Published: 2 March 2023

1. Introduction

People are paying more and more attention to drug quality and safety, and the pharmaceutical industry has become one of the most regulated industries [1]. Since the World Health Organization (WHO) first implemented good manufacturing practice of medical products (GMP) in the 1960s, the rules and regulations of various countries for drug safety production have been continuously improved and adjusted [2], and the International Conference on Harmonization (ICH) proposed the guideline for metallic impurities (Q3D) to ensure the quality of drugs [3].

The application of metal catalysts in drug synthesis is becoming more and more general, resulting in the residue of heavy metals in the final product [4]. For example, palladium carbon and Raney nickel are employed in the synthesis of mepivacaine hydrochloride and rivaroxaban, respectively, and the bentonite loaded with $CuCl_2$ is used as the catalyst in the synthesis of aspirin [5–7]. Furthermore, concentrated sulfuric acid or phosphoric acid is often also used as a catalyst in the industrial production of aspirin [8]. The corrosive properties of these two acids can leach metals such as copper from stainless steel equipment into the drug [9]. At present, heavy metal pollution in water has become a global environmental problem. ICH-Q3D stipulates that the permitted daily exposure (PDE) of copper is 3 mg/day (assumes 10 g oral or parenteral dose) [10]. Heavy metals such as Cu, Pb, Hg, Zn, etc., have obvious effects on human metabolism and normal physiological functions [11]. For example, heavy metals can cause harm to mental and central nervous function, lungs, kidneys, and other organs [12–14]. If copper in the human body exceeds the standard, it can cause symptoms such as nausea and vomiting, abdominal pain and diarrhea, and acute hepatotoxicity [15,16]. Alzheimer's disease (AD) is also related to the imbalance of copper in the body [17,18]. On the other hand, heavy metals can have adverse effects on the ecological environment. When released into the environment, they do not

biodegrade and instead accumulate through the food chain. It has been reported that heavy metals are highly toxic and most of them even cause cancer [19,20].

At present, the methods of removing heavy metals mainly include alcohol precipitation, molecular imprinting, superfluid, and adsorption, etc. [21,22]. There are many methods to remove heavy metal pollution which have problems such as high treatment cost, difficult reuse, complicated process, and may also produce secondary pollution and waste water resources. In contrast, the adsorption method has advantages such as wide application range, fast reaction speed, adaptability to different reaction conditions, and environmental friendliness, which have attracted high attention from researchers. Commonly employed adsorbents are hydrogel [23], cation exchange resin [24], zeolite [25], and acticarbon [26], etc. The exchangeable cations in zeolite skeleton can exchange with heavy metals in water, and the large specific surface area has a unique adsorption function for heavy metals [27]. Therefore, zeolite has been drawing much attention because of its low price, unique mechanical stability, and fast regeneration speed [28]. Olegario, etc., found that Philippine natural zeolite showed good adsorption capacity and ion selectivity for heavy metals such as As^{5+}, Cu^{2+}, and Ni^{2+} [29]. Fan's team found that the maximum adsorption capacity of NaX zeolite for Cd^{2+}, Cu^{2+}, and Pb^{2+} reached 2.14, 1.87, and 2.38 mmol g^{-1}, respectively [30]. The tetrahedrons of silica and alumina in zeolite are connected to the pores by sharing all oxygen atoms, forming a three-dimensional network structure. The Na^{+}, K^{+}, and Ca^{+} ions present in the structural channels of zeolite can be replaced by other metal cations such as Cu^{2+}, Pb^{2+}, Zn^{2+}, and Cd^{2+}, causing heavy metals in the water to adsorb on the zeolite, while the zeolite structure remains almost unchanged [31]. The exchangeable cations in zeolite skeleton can exchange with heavy metals in water. The large specific surface area and three-dimensional pore structure of zeolite make it widely used in the process of metal ion adsorption and removal. However, nanomaterials are difficult to separate from the mother liquor after adsorption, which restricts their practical application.

Membrane adsorption technology possesses both adsorption and filtration functions and is widely used in water treatment, drug purification, chemical industry, and other fields [32]. Yurekli et al. dispersed zeolite in polysulfone to make a mixed matrix membrane (MMM) and the adsorption capacity of Ni^{2+} and Pd^{2+} was 122 and 682 mg g^{-1}, respectively [33]. However, the coating of the zeolite by the polymer can lead to a longer equilibrium time. In addition, the adsorbent may fall off from the membrane during the adsorption/desorption process, resulting in secondary pollution [34]. The sandwich adsorption membrane is composed of three parts: the base membrane, adsorption layer, and surface layer. First, the nylon microfiltration membrane is used as the base membrane to filter the adsorbent particles, and then the adsorption layer of micron thickness is obtained. Finally, the hydrophilic polymer solution is scraped and coated on the surface of the adsorption layer, and the asymmetric porous polymer surface membrane was obtained by the immersion precipitation phase conversion method.

The sandwich membrane structure has the following advantages: 1. The polymer solution can penetrate into the microporous membrane where there is no adsorbent at the edge of the membrane, playing the anchoring role and improving the strength and stability of the membrane. 2. The nanoparticles are fixed between the base membrane and the surface layer to avoid secondary pollution caused by the adsorbent falling off. 3. The adsorbent nanoparticles were prepared in a sandwich membrane, which improved the adsorption efficiency and was easily separated from the mother liquor and easy to recover. 4. The cation exchange property of zeolite makes the metal ions adsorbed, and drug molecules pass through the gap of nanoparticles without passing through the three-dimensional pore of zeolite, so as to achieve the purpose of separating drugs and heavy metals, which is conducive to industrial applications. In this paper, NaY zeolite was synthesized by a hydrothermal method and used as an adsorbent to prepare the sandwich adsorptive membrane. The kinetics, adsorption isotherm, dynamic adsorption, and reusability for

Cu^{2+} adsorption were studied, and the dynamic adsorption of Cu^{2+} in aspirin aqueous solution was conducted.

2. Experimental Part

2.1. Materials

Sodium hydroxide (NaOH) and hydrochloric acid (HCl) were bought from Jinan Jiewei Chemical Technology Co., Ltd., Jinan, China. N-methylpyrrolidone (NMP) and ethanol (EtOH) were bought from Shanghai Gaoshen Chemical Co., Ltd., Shanghai, China. Sodium metaaluminate ($AlNaO_2$) and sodium silicate solutions were all analytical reagents and bought from Shanghai McLean Biochemical Technology Co., Ltd., Shanghai, China. Aspirin was purchased from China National Pharmaceutical Group Co., Ltd., Beijing, China. Copper standard solution was bought from Beijing Zhongke Quality Control Technology Co., Ltd., Beijing, China. Sodium chloride (NaCl) was purchased from Tianjin Zhiyuan Chemical Reagent Co., Ltd., Tianjin, China. Polyethersulfone (PES) was bought from Shanghai Zhuoying plasticization Co., Ltd., Shanghai, China, and nylon membranes (Φ25 mm) were purchased from Dalian Shizhou Filter Equipment Co., Ltd., Dalian, China.

2.2. Preparation of NaY Zeolite

NaY zeolite was preparation by a hydrothermal method [35] with a molar composition of 12.8 (Al_2O_3):17.1 (Na_2O_3):1 (SiO_2):675 (H_2O). During this procedure, the identified amounts of NaOH, $AlNaO_2$, and DI water were mixed; then, sodium silicate solutions were added drop-wise and stirred until completely dissolved. After aging for 12 h, the mixture was moved to a polytetrafluoroethylene (PTFE) bottle and then kept at 90 °C for 12 h. After it cooled down, the solid was filtered and washed with DI water.

2.3. Preparation of PES-SPES/NaY Zeolite/Nylon Sandwich Adsorptive Membrane

SPES was synthesized according to the reference [36,37]. The nylon membrane (Φ 25 mm) was soaked in EtOH for 2 min and washed with DI water. Then, 100 mg NaY zeolite was dispersed in 100 mL EtOH and ultrasoniced for 10 min. A certain volume of the suspension was filtered with the nylon membrane to obtain the NaY zeolite/nylon membrane. Finally, the NMP casting solution of SPES-PES (10 wt%, SPES/PES = 1/4) was casted on the NaY zeolite/nylon membrane with a scraper (spacing of 365 μm), then soaked in pure water for 8 h to obtain the PES-SPES/NaY zeolite/nylon sandwich adsorptive membrane (Figure 1). The sandwich adsorption membrane is composed of three parts: the base membrane (nylon membrane), adsorption layer (NaY zeolite), and surface layer (PES-SPES hydrophilic polymer layer).

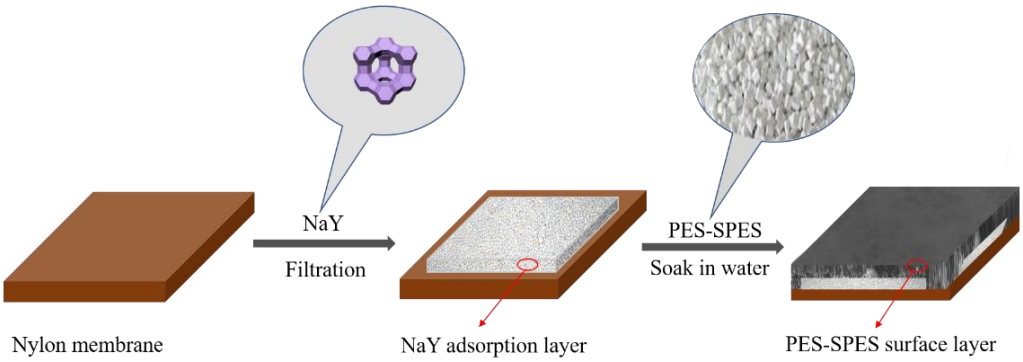

Figure 1. Schematic diagram of the preparation of PES-SPES/NaY zeolite/nylon sandwich adsorptive membrane.

2.4. Static Adsorption

The adsorption performance of the sandwich adsorption membrane was investigated by the stirring method. The concentration of Cu^{2+} aqueous solution (100 mL) was prepared

in the conical flask, and the adsorption membrane was added. The pH value of the aqueous solution was adjusted by 0.1 mol·L^{-1} HCl and 0.1 mol·L^{-1} NaOH. The concentration of Cu^{2+} in the conical flask solution was measured at room temperature by stirring at a low speed (40 rpm) under the action of a magnetic agitator. The saturated adsorption capability (Q_e, mg g^{-1}) was expressed as Equation (1):

$$Q_e = \frac{c_0 - c_e}{\Delta m} \times v \quad (1)$$

where c_e and c_0 are the saturated and initial concentrations of Cu^{2+} solution (mg L^{-1}), respectively, Δm is the mass of NaY zeolite (g), and v is the volume of aqueous solution (L). The removal ratio (Re, %) and desorption ratio (DR, %) were calculated as Equations (2) and (3), respectively:

$$Re = \frac{c_0 - c_e}{c_0} \times 100\% \quad (2)$$

$$DR = \frac{c_1 \times v_1}{(c_0 - c_e) \times v} \quad (3)$$

where v_1 and c_1 are the volume of eluent (L) and the concentration of Cu^{2+} in the eluent (mg L^{-1}), respectively.

2.5. Dynamic Adsorption and Desorption

During the dynamic filtering experiment, the sandwich membrane (Φ 25 mm) was transferred to the filter, pre-treated with 20 mL pure water, and then the Cu^{2+} solution was flowed through the sandwich adsorptive membrane with the rate of 0.68 mL min^{-1}. During the desorption experiment, the eluent (saturated NaCl solution) was filtered at a rate of 0.8 mL min^{-1} [38]. The pure water flux was expressed as Equation (4) [39]:

$$J_0 = \frac{V}{A \times \Delta t \times P} \quad (4)$$

where Δt is the filtration time (h), V and A are the volume of filtered water (L) and the effective area (m^2), respectively, and J_0 and P are the pure water flux (L m^{-2} h^{-1} bar^{-1}) and test pressure (1 bar = 100 KPa).

2.6. Characterization

The structures and morphologies of ZaY particles and the sandwich membrane were under observation by field emission scanning electron microscope (SEM, S-480003040155, Hitachi, Tokyo, Japan). The membrane structures were investigated by viewing the surface and cross section of the sandwich membrane. The membrane was freeze dried in liquid nitrogen and then quenching to observe the cross section of the membrane. Quantitative analysis of Cu^{2+} in water (λ_{max} = 547 nm) was measured by the colorimetric method with a UV-vis spectrophotometer (UV, Lambda 35, PerkinElmer, Waltham, MA, USA) [40]. The pore characteristics and BET surface areas of the samples were determined using N^2 adsorption/desorption analysis performed at 200 °C on a specific surface area analyzer (BSD-660, BSD Instrument, Beijing, China). Specimens of the zeolites were measured by an X-ray powder diffraction technique (XRD, XRD-6000, Shimadzu, Kyoto, Japan).

3. Results and Discussion

3.1. Characterization of Sandwich Membrane

Figure 2 shows the SEM images of the sandwich adsorptive membrane clearly. The surface is smooth and contains a large number of nanopores (Figure 2b), which can filter out the impurities in the solution and prevent blocking of the membrane. The PES-SPES layer has a finger-like asymmetrical cross section to reduce flow resistance during filtration. The total thickness of the sandwich adsorptive membrane is 129.5 μm, and the thickness of

the PES-SPES polymer layer and substrate membrane are 32.3 μm and 78.9 μm, respectively. The adsorbent layer forms a compact particle accumulation with a thickness of 18.3 μm. The total mass of the membrane is 52.0 mg, and the percentage of adsorbent in the total mass of the membrane is 7.7 wt%. The water flux of the sandwich adsorptive membrane is 47.2 L m^{-2} h^{-1} bar^{-1}. Figure 2d is the characterization of NaY zeolite. The XRD pattern is consistent with the Y-type zeolite (2θ = 6.2°, 15.6°, 23.6°, and 31.36°) [41]; the crystal is uniform, with a diameter of approximately 0.84 μm.

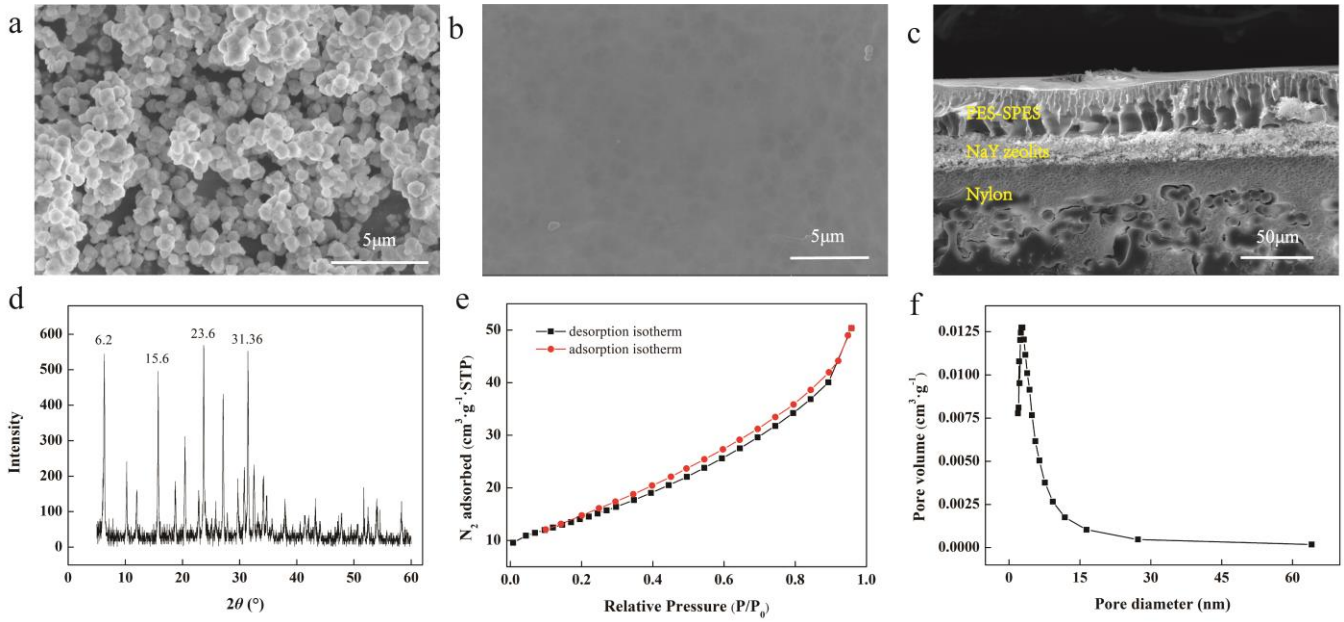

Figure 2. (**a**) SEM images of NaY zeolite; (**b**) surface SEM images of the sandwich adsorptive membranes; (**c**) cross−section SEM images of the sandwich adsorptive membranes; (**d**) XRD of NaY zeolite; (**e**) N_2 adsorption and desorption curves of the sandwich adsorptive membranes; (**f**) the curves of pore diameter distribution of the sandwich adsorptive membranes.

Figure 2e shows the N_2 adsorption/desorption isotherm of the sandwich adsorptive membrane. The adsorption branch and desorption branch in the curve do not coincide, forming a narrow hysteresis ring, indicating that there is a mesoporous structure in the membrane [42]. The BET specific surface area is 50.9 m^2 g^{-1}. Figure 2f displays the pore size distribution curve of the sandwich adsorptive membrane. The pore diameter is mostly distributed within the scope of 2–10 nm, with an average size of 6.6 nm (in the range of mesoporous pore) [43].

3.2. Adsorption Isotherm

To explore the effect of pH, sandwich adsorptive membranes were added to 5 mg L^{-1} of Cu^{2+} aqueous solution (100 mL) with different pH (2.0, 3.0, 4.0, 5.0, and 6.0) at room temperature under stirring (40 rpm). It can be seen from Figure 3a that the Q_e of the sandwich adsorptive membrane was obviously affected by the solution pH. With the increase in pH from 2.0 to 6.0, the Q_e increased significantly from 0 to 71.75 mg g^{-1}. NaY is a kind of porous aluminum silicate material with a three−dimensional pore structure. Na^+ and K^+ in its skeleton are the main exchangeable cations, and it is easy to have ion exchange with other cations in aqueous solution. In acidic water, a large amount of H^+ will form ionic competition with Cu^{2+}, resulting in the reduction in adsorption capacity [44]. With the increase in pH, the competition between H^+ and Cu^{2+} is gradually weakened, and the adsorption capacity of Cu^{2+} increases gradually, reaching the maximum at pH 6.0. With the increase in pH, the Q_e gradually increases. In order to avoid the hydrolysis of Cu^{2+} under alkaline conditions or neutral, pH = 6.0 was chosen as the optimal reaction condition.

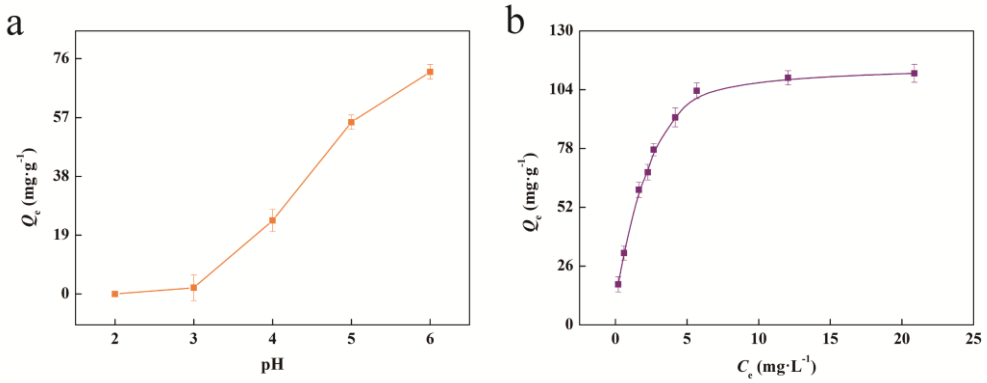

Figure 3. (**a**) Influence of pH values on adsorption capacity; (**b**) The adsorption kinetic curves of sandwich adsorptive membrane for Cu^{2+}.

The sandwich adsorptive membrane (containing 4 mg adsorbent) was placed in Cu^{2+} aqueous solution (100 mL) with different concentrations of 1, 2, 4, 5, 6, 8, 10, 16, and 16 mg L^{-1}, respectively (pH 6.0, 25 °C), for 8 h. As shown in Figure 3b, with the increase in Cu^{2+} aqueous concentration (c_e), the adsorption capacity of Cu^{2+} on the sandwich adsorption membrane also increases, and the growth trend shows that the adsorption capacity of Cu^{2+} rises rapidly first and then gradually flattens. This may be due to the limited ions available for exchange in NaY zeolite, and the adsorption capacity reaches the maximum when the concentration of Cu^{2+} solution reaches a certain amount. In order to explain the adsorption mechanism of the sandwich adsorptive membrane toward Cu^{2+}, the adsorption isotherms date was fitted to Freundlich, Langmuir, and D-R adsorption models [45–47]. The Langmuir adsorption model indicates that the adsorption processes are chemical adsorption and monolayer adsorption, and there are limited homogeneous adsorption sites. The Freundlich adsorption isotherm model is fit for multilayer adsorption, and calculated by the following Equations (5) and (6):

$$Q_e = k_F c_e^{\frac{1}{a}} \tag{5}$$

$$\log Q_e = \log k_F + \frac{1}{a} \log c_e \tag{6}$$

where k_F is the Freundlich parameter (mg g^{-1}) (L $mg^{-1})^{1/a}$, indicating the affinity between adsorbents and adsorbents, and a is the adsorption strength [45]. The Langmuir adsorption isotherm model is based on chemisorption monolayer and expressed as Equation (7):

$$\frac{1}{Q_e} = \frac{1}{Q_m} + \frac{1}{bQ_m}\frac{1}{c_e} \tag{7}$$

where b and Q_m are the Langmuir parameter (L mg^{-1}) and the saturated adsorption capacity (mg g^{-1}), respectively, and b reflects the stability of the combination of adsorbent and adsorbate [46]. It can be seen from Figure 4 and Table 1 that the Langmuir adsorption isotherm model ($R^2 > 0.974$) displays a more satisfactory description than the Freundlich adsorption isotherm model, which indicates that the adsorption of Cu^{2+} on the sandwich adsorptive membrane is chemical adsorption, and the Q_m of 111.3 mg g^{-1} is higher than that recorded in the other literatures (Table 2). To further describe the adsorption mechanism, the D-R model is analyzed as Equations (8)–(11) to evaluate the average adsorption energy:

$$Q_e = Q_m exp(-k\varepsilon^2) \tag{8}$$

$$lnQ_e = lnQ_m - k\varepsilon^2 \tag{9}$$

$$\varepsilon = RTln(1 + \frac{1}{c_e}) \tag{10}$$

$$E = \frac{1}{(2k)^{1/2}} \tag{11}$$

where ε is the Polanyi potential, and R and T are the ideal gas parameter (8.314 kJ mol^{-1} K^{-1}) and the degree kelvin (K), respectively. The average adsorption free energy (E, kJ mol^{-1}) is used to judge whether the adsorption is physical adsorption or ion exchange adsorption [47]. As shown in the Table 1, E is 15.77 kJ mol^{-1}, between 8–16 kJ mol^{-1}, proving that is an ion exchange process [48]. Metal cations enter the three-dimensional pore of the zeolite skeleton and exchange with the cations of the zeolite skeleton itself.

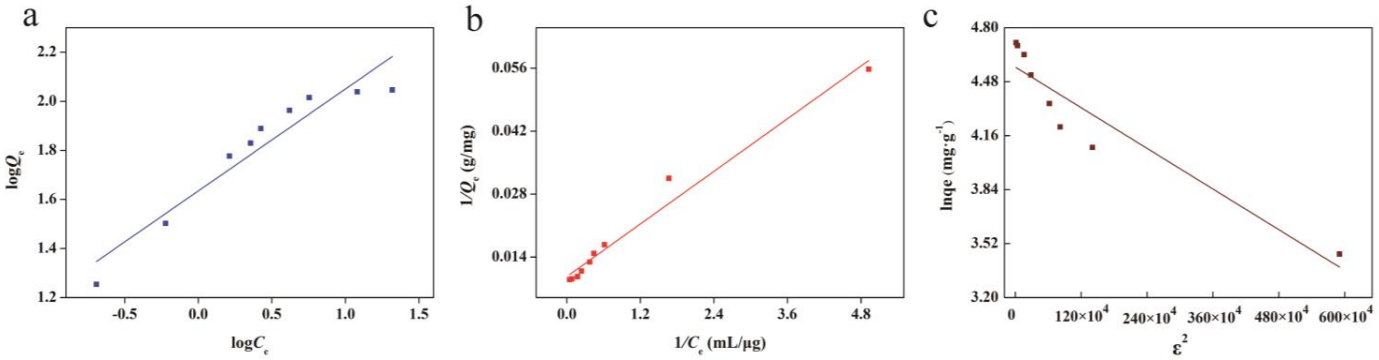

Figure 4. Static adsorption thermodynamics: (**a**) The fitting curve of Freundlich model; (**b**) The fitting curve of Langmuir model; (**c**) The fitting curve of D−R model.

Table 1. Adsorption isotherm parameter for Cu^{2+} adsorption on sandwich adsorptive membrane.

Isotherm Model	Parameters	–
Freundlich	1/a	0.5792
	k_F (mg g^{-1}) (L mg^{-1})$^{1/n}$	2.976
	R^2	0.899
Langmuir	Q_m (mg g^{-1})	111.3
	b (L mg^{-1})	0.922
	R^2	0.974
D-R	k	0.00201
	E (kJ mol^{-1})	15.77
	R^2	0.869

Table 2. Comparison of Cu^{2+} adsorption by different adsorbents.

Adsorbents	Concentrations (mg L^{-1})	Adsorption Time (min)	Saturated Adsorption Capacity (mg g^{-1})	Reference
Natural zeolites from the Philippines	136	360	14.65	[29]
bagasse pith grafted copolymer (BPGC)	6	700	105	[49]
Chitosan/hydroxyapatite/nano-magnetite (Fe_3O_4) composite	1–5	100	3.65	[50]
Chitosan blended with polyvinyl alcohol (PVA) membrane	20–100	720	35.71	[51]
PES-SPES/NaY zeolite/nylon sandwich membrane	1–25	480	111.3	This work

3.3. Adsorption Kinetics

The kinetics of the sandwich adsorptive membrane were conducted in Cu^{2+} aqueous solution (5, 10 mg L^{-1}, pH 6.0, 100 mL) under stirring (40 rpm) at room temperature. Figure 5a shows the change curve of the adsorption capacity with time. It can be seen that,

with the growing time (0–300 min), the adsorption capacity increases rapidly with time. This is because there are more exchangeable Na^+ and K^+ ions in the NaY zeolite skeleton at the initial stage of adsorption. Then, the NaY zeolite skeleton exchangeable ions gradually become less, so the adsorption capacity growth rate also becomes slow, until it reaches a stable rate.

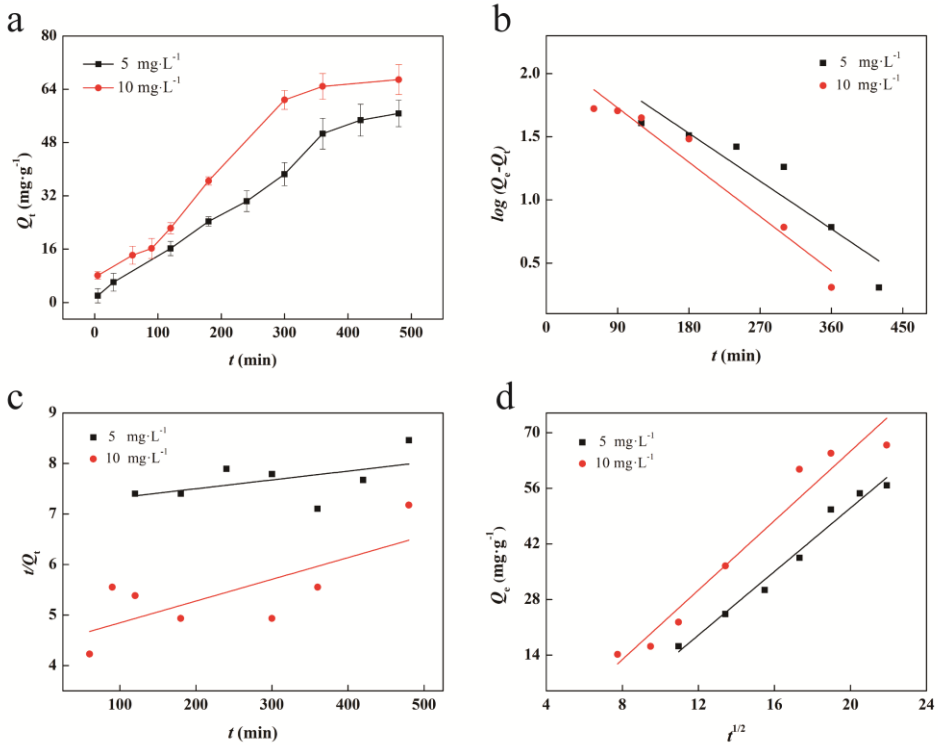

Figure 5. (**a**) Adsorption capacity with time of membrane at different concentrations; (**b**) Linear fitting of the pseudo−first−order model; (**c**) Linear fitting of the pseudo−second−order model; (**d**) Linear fitting of the intra-particle diffusion model.

In order to clarify the control mechanism and velocity limiting steps in the adsorption process, three commonly used kinetic models were selected to analyze the experimental data. The pseudo-first-order adsorption kinetics model represents the adsorption reaction caused by boundary diffusion, and the pseudo-second-order adsorption kinetics model represents the adsorption process controlled by chemisorption, and expressed as Equations (12) and (13), respectively [52]:

$$\log(Q_e - Q_t) = \log Q_e - \frac{k_1 t}{2.303} \tag{12}$$

$$\frac{t}{Q_t} = \frac{1}{k_2 Q_e{}^2} + \frac{t}{Q_e} \tag{13}$$

where Q_t (mg g^{-1}) is the adsorption capacity at a time t, and k_2 (g mg^{-1} min^{-1}) and k_1 (min^{-1}) are the pseudo-second-order and pseudo-first-order rate parameter, respectively. The model of intra-particle diffusion is commonly used to describe the rate-limiting step in the adsorption process [53] and expressed as Equation (14):

$$Q_t = k_i t^{\frac{1}{2}} + C \tag{14}$$

where C (mg g^{-1}) is the intercept of the curve in the graph and k_i is the diffusion rate parameter (mg g^{-1} $min^{-1/2}$). Table 3 shows that the R^2 of pseudo-first-order kinetics is preferable to the pseudo-second-order kinetics at different initial concentrations (5 and 10 mg L^{-1}) and indicates that the rate-controlling step is the transport of Cu^{2+} to the

membrane surface [27]. The fitting line of Q_t vs. $t^{1/2}$ does not pass through the origin in Figure 5d, indicating that intra-particle diffusion is not the only rate-limiting process of Cu^{2+} adsorption by the sandwich adsorptive membrane and that the effects of surface diffusion are also important [54].

Table 3. Kinetic adsorption model parameters of Cu^{2+} by sandwich adsorptive membrane.

Kinetic Models	Parameters	5 mg L^{-1}	10 mg L^{-1}
The pseudo first order	Slope	−0.0042	−0.0048
	Intercept	2.286	2.160
	k_1 (min^{-1})	0.0097	0.011
	R^2	0.850	0.941
The pseudo second order	Slope	0.0017	0.0043
	Intercept	7.151	4.416
	k_2 (g mg^{-1} min^{-1})	4.04×10^{-7}	4.20×10^{-6}
	R^2	0.120	0.454
Intra-particle diffusion model	Slope (k_i (mg g^{-1} $min^{-1/2}$))	4.005	4.371
	Intercept (C (mg g^{-1}))	−29.028	−22.071
	R^2	0.974	0.949

3.4. Dynamic Adsorption and Desorption

During dynamic adsorption, 10 mg L^{-1} and 5 mg L^{-1} Cu^{2+} aqueous solutions (100 mL, pH 6.0) were filtered with the sandwich membrane at 25 °C. As shown in Figure 6a, for 5 mg L^{-1} Cu^{2+} aqueous solution, in the initial process (v < 7.8 mL), $c/c_0 = 0$, indicating that all Cu^{2+} are adsorbed; then, c/c_0 increases rapidly, and tends to be stable. For 10 mg·L^{-1}, the adsorption curve grows faster when the filtration volume is less than 30 mL, and then the growth rate slows down and gradually reaches equilibrium. $c/c_0 = 0.8$ and $c/c_0 = 0.1$ are the saturation point and breakthrough point, respectively, and the corresponding solution volumes are the saturation volume (v_s) and breakthrough volume (v_b), respectively [55]. v_s and v_b are 60.2 and 9.4 mL, respectively. For the 10 mg L^{-1} Cu^{2+} aqueous solution, v_s and v_b are 33.6 and 2.6 mL, respectively. The dynamic adsorption capacity (DC) is calculated by the following Equation (15):

$$DC = \frac{\int_0^v (c_0 - c)dv}{\Delta m} \quad (15)$$

where c is the concentration of Cu^{2+} in the filtrate (mg L^{-1}), and v is the filtration volume (L). The $DC_{0.1}$ and $DC_{0.8}$ of the membrane are 1.80, 24.05 mg g^{-1} for the 5 mg L^{-1} Cu^{2+} solution, and 2.25 and 35.53 mg g^{-1} for the 10 mg L^{-1} Cu^{2+} solution, respectively, indicating that the sandwich membrane has good adsorption capacity for Cu^{2+}.

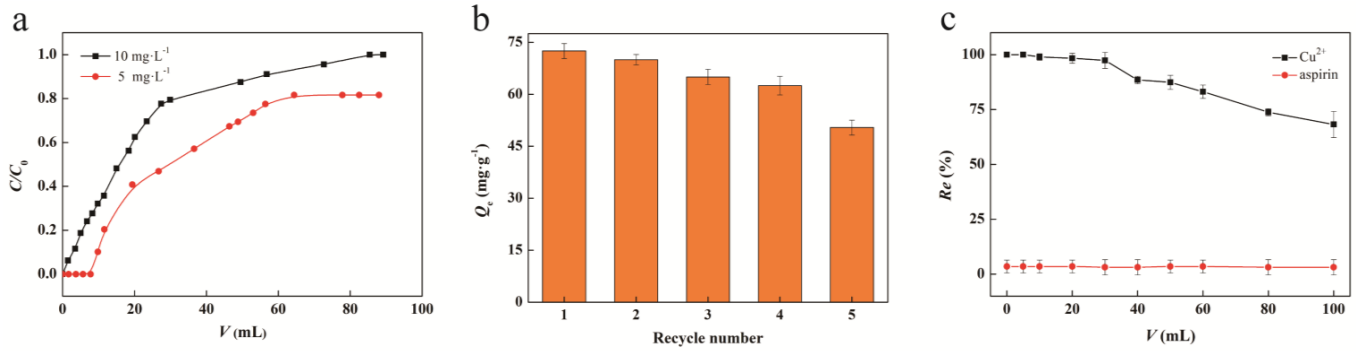

Figure 6. Dynamic adsorption of sandwich membrane: (**a**) Breakthrough curves; (**b**) Recycle numbers of membrane; (**c**) Dynamic adsorption of sandwich membrane in aspirin−Cu^{2+} mixed solution.

In industrial production, the reusability of the membrane is very important; the excellent performance of the membrane can save production costs and greatly improve

economic benefits. The reusability of the sandwich adsorptive membrane was investigated by a dynamic adsorption/desorption experiment. A total of 5 mg L^{-1} Cu^{2+} aqueous solutions (100 mL, pH 6.0) was filtered with the sandwich membrane at 25 °C at a rate of 0.68 mL min^{-1}. After adsorption, 20 mL saturated NaCl solution was filtered as eluent at a rate of 0.25 mL min^{-1}, and then 10 mL DI water was filtered to remove the residual NaCl for the next cycle. It can be seen from Figure 6b that the Q_e in the five cycles are 72.5, 70.0, 65.3, 62.5, and 50.4 mg g^{-1}, respectively, indicating that the sandwich membrane has good regeneration and reuse performance.

In order to meet the standards of GMP and ICH for trace meta l impurities in drugs, the mixed aqueous solution (100 mL, pH 6.0) of aspirin (20 mg L^{-1}) and Cu^{2+} (1 mg L^{-1}) was filtered with the sandwich adsorptive membrane at 25 °C. As shown in Figure 6c, the removal ratio of Cu^{2+} by the sandwich adsorptive membrane reaches 100% when $v < 10$ mL, complying with the ICH-Q3D standard (PDE $\leq$ 3 mg·day^{-1}); then, the removal ratio decreases gradually with the increased volume, and remains above 70% when $v < 100$ mL. On the contrary, the removal ratio of aspirin is almost zero, indicating that the sandwich adsorptive membrane can effectively remove Cu^{2+} from the aspirin solution. Aspirin has a large molecular diameter and exists as an anion in water, so it cannot be exchanged with the cation in the zeolite skeleton, thus achieving a good separation effect with Cu^{2+}.

4. Conclusions

PES-SPES/NaY zeolite/nylon sandwich adsorptive membranes were successfully fabricated. It can be observed that the base membrane plays a supporting role, the adsorption layer ensures sufficient adsorption capacity, and the surface layer makes the membrane more stable. The Langmuir isotherm model, D-R isotherm model, and the pseudo-first-order kinetic model can well represent the adsorption of Cu^{2+} on the membrane, indicting a chemisorption adsorption and ion exchange reaction process, with the maximum adsorption capacity of 111.25 mg·g^{-1}. The sandwich adsorptive membranes exhibited good reusability in the cycling test. Contrary to the adsorption mechanism of Cu^{2+}, the diameter of aspirin molecules is large, and they cannot be allowed to enter the nanoparticle gap. Moreover, it ionizes into anion form in water and cannot exchange with the cation in the NaY zeolite skeleton. Therefore, it is of guiding significance to apply the three-dimensional nanomaterials in the separation of heavy metals in drugs.

Author Contributions: Y.G. and X.Z.: conceptualization, investigation, writing—original draft, writing—editing; Y.X. and Y.H.: investigation, supervision, writing—review; Z.J.: conceptualization, supervision, writing—review; Y.M. and X.W.: investigation, writing—original draft, writing—editing. All authors have read and agreed to the published version of the manuscript.

Funding: This work was supported by Natural Science Foundation Steel and Iron Foundation of Hebei Province of China (No. B2020209022), National Natural Science Foundation of China (No. 51920105012) and PhD Startup Program of North China University of Science and Technology (No. BS2017031).

Data Availability Statement: No data were used for the research described in the article.

Conflicts of Interest: The authors declare that they have no known competing financial interest or personal relationships that could have appeared to influence the work reported in this paper.

References

1. Rahman, N.; Azmi, S.N.H.; Wu, H.-F. The importance of impurity analysis in pharmaceutical products: An integrated approach. *Accredit. Qual. Assur.* **2006**, *11*, 69–74. [CrossRef]
2. Tabersky, D.; Woelfle, M.; Ruess, J.-A.; Brem, S.; Brombacher, S. Recent regulatory trends in pharmaceutical manufacturing and their impact on the industry. *Chimia* **2018**, *72*, 146–150. [CrossRef] [PubMed]
3. Wollein, U.; Bauer, B.; Habernegg, R.; Schramek, N. Potential metal impurities in active pharmaceutical substances and finished medicinal products—A market surveillance study. *Eur. J. Pharm. Sci.* **2015**, *77*, 100–105. [CrossRef] [PubMed]
4. Rao, R.N.; Talluri, M.K. An overview of recent applications of inductively coupled plasma-mass spectrometry (ICP-MS) in determination of inorganic impurities in drugs and pharmaceuticals. *J. Pharm. Biomed. Anal.* **2007**, *43*, 1–13. [CrossRef]

5. Abdullaev, M.G. Kinetics of one-step mepivacaine synthesis on polymers containing Pd-nanoparticles. *Pharm. Chem. J.* **2019**, *52*, 865–867. [CrossRef]
6. Tian, S.X.; Tang, B.; Zhang, M.Z.; Gao, Q.J.; Chen, B. An improved synthesis of rivaroxaban. *Org. Prep. Proced. Intern.* **2017**, *49*, 169–177. [CrossRef]
7. Min, Y.; Shi, F.G. The Preparation and characterization of zinc chloride-loaded bentonite solid acid catalyst. *J. Yunnan Natl. Univ.* **2007**, *2*, 168–171.
8. Bamoharram, F.F.; Heravi, M.M.; Roshani, M.; Gharib, A.; Jahangir, M. Catalytic method for synthesis of aspirin by a green, efficient and recyclable solid acid catalyst (Preyssler's Anion) at Room Temperature. *J. Chin. Chem. Soc.* **2013**, *54*, 1017–1020. [CrossRef]
9. Sharma, A.; Jain, S.K. Elemental impurities in drug product. *Int. J. Pharm. Sci. Res.* **2017**, *2*, 31–38.
10. Pohl, P.; Bielawska-Pohl, A.; Dzimitrowicz, A.; Jamroz, P.; Welna, M. Impact and practicability of recently introduced requirements on elemental impurities. *Trac Trends Anal. Chem.* **2018**, *101*, 43–55. [CrossRef]
11. Cheraghi, M.; Lorestani, B.; Yousefi, N. Effect of waste water on heavy metal accumulation in hamedan province vegetables. *Int. J. Bot.* **2009**, *5*, 190–193. [CrossRef]
12. Reglero, M.; Taggart, M.; Lidia, M.; Rafael, M. Heavy metal exposure in large game from a lead mining area: Effects on oxidative stress and fatty acid composition in liver. *Environ. Pollut.* **2009**, *157*, 1388–1395. [CrossRef] [PubMed]
13. Kampa, M.; Castanas, E. Human health effects of air pollution. *Environ. Pollut.* **2008**, *151*, 362–367. [CrossRef] [PubMed]
14. Gybina, A.A.; Prohaska, J.R. Copper deficiency results in AMP-activated protein kinase activation and acetylCoA carboxylase phosphorylation in rat cerebellum. *Brain Res.* **2008**, *1204*, 69–76. [CrossRef]
15. Araya, M.; McGoldrick, M.C.; Klevay, L.M.; Strain, J.; Robson, P.; Nielsen, F.; Olivares, M.; Pizarro, F.; Johnson, L.; Poirier, K.A. Determination of an acute no-observed-adverse-effect level (NOAEL) for copper in water. *Regul. Toxicol. Pharmacol.* **2001**, *34*, 137–145. [CrossRef] [PubMed]
16. Chuttani, H.; Gupta, P.; Gulati, S.; Gupta, D. Acute copper sulfate poisoning. *Am. J. Med.* **1965**, *39*, 849–854. [CrossRef] [PubMed]
17. Nuttall, J.R.; Oteiza, P.I. Zinc and the aging brain. *Genes Nutr.* **2014**, *9*, 379. [CrossRef] [PubMed]
18. Faller, P. Copper in Alzheimer disease: Too much, too little, or misplaced? *Free. Radic. Biol. Med.* **2012**, *52*, 747–748. [CrossRef]
19. Afroze, S.; Sen, T.K. A Review on heavy metal ions and dye adsorption from water by agricultural solid waste adsorbents. *Water Air Soil Pollut.* **2018**, *229*, 225. [CrossRef]
20. Cocâr, D.; Deac, A. Carcinogenic risk evaluation for human health risk assessment from soils contaminated with heavy metals. *Int. J. Environ. Sci. Technol.* **2016**, *13*, 2025–2036. [CrossRef]
21. Stewart, M.P.; Langer, R.; Jensen, K.F. Intracellular delivery by membrane disruption: Mechanisms, strategies, and concepts. *Chem. Rev.* **2018**, *118*, 7409–7531. [CrossRef] [PubMed]
22. Yang, J.; Hou, B.; Wang, J.; Tian, B.; Bi, J.; Wang, N.; Li, X.; Huang, X. Nanomaterials for the removal of heavy metals from wastewater. *Nanomaterials* **2019**, *9*, 424. [CrossRef]
23. Yao, G.; Li, S.; Xu, J.; Liu, H. Dual-Responsive Graphene Oxide/Poly(NIPAM-*co*-AA) Hydrogel as an Adsorbent for Rhodamine B and Imidacloprid. *J. Chem. Eng. Data* **2019**, *64*, 4054–4065. [CrossRef]
24. Demirbas, A.; Pehlivan, E.; Fethiye, G.; Turkan, A.; Gulsin, A. Adsorption of Cu(II), Zn(II), Ni(II), Pb(II), and Cd(II) from aqueous solution on Amberlite IR-120 synthetic resin. *J. Colloid Interface Sci.* **2005**, *282*, 20–25. [CrossRef] [PubMed]
25. Peri, J.; Trgo, M.; Medvidovi, N.V. Removal of zinc, copper and lead by natural zeolite-A comparison of adsorption iso-therms. *Water Res.* **2004**, *38*, 1893–1899. [CrossRef] [PubMed]
26. Ghaedi, M.; Nasab, A.G.; Khodadoust, S.; Rajabi, M.; Azizian, S. Application of activated carbon as adsorbents for efficient removal of methylene blue: Kinetics and equilibrium study. *J. Ind. Eng. Chem.* **2014**, *20*, 2317–2324. [CrossRef]
27. Cheng, T.H.; Sankaran, R.; Show, P.L.; Ooi, C.W.; Liu, B.L. Removal of protein wastes by cylinder-shaped NaY zeolite ad-sorbents decorated with heavy metal wastes. *Int. J. Biol. Macromol.* **2021**, *185*, 761–772. [CrossRef]
28. Coronas, J. Present and future synthesis challenges for zeolites. *Chem. Eng. J.* **2010**, *156*, 236–242. [CrossRef]
29. Olegario, E.; Pelicano, C.M.; Felizco, J.C.; Mendoza, H. Thermal stability and heavy metal (As^{5+}, Cu^{2+}, Ni^{2+}, Pb^{2+} and Zn^{2+}) ions uptake of the natural zeolites from the Philippines. *Mater. Res. Express* **2019**, *6*, 085204. [CrossRef]
30. Fan, X.; Liu, H.; Anang, E.; Ren, D. Effects of electronegativity and hydration energy on the selective adsorption of heavy metal ions by synthetic NaX zeolite. *Materials* **2021**, *14*, 4066. [CrossRef]
31. Zhao, Y. Review of the natural, modified, and synthetic zeolites for heavy metals removal from wastewater. *Environ. Eng. Sci.* **2016**, *33*, 443–454.
32. Abdullah, N.; Yusof, N.; Lau, W.J.; Jaafar, J.; Ismail, A.F. Recent trends of heavy metal removal from water/wastewater by membrane tech-nologies. *J. Ind. Eng. Chem.* **2019**, *76*, 17–38. [CrossRef]
33. Yurekli, Y. Removal of heavy metals in wastewater by using zeolite nano-particles impregnated polysulfone membranes. *J. Hazard. Mater.* **2016**, *309*, 53–64. [CrossRef] [PubMed]
34. Hao, S.; Jia, Z.; Wen, J.; Li, S.; Peng, W.; Huang, R.; Xu, X. Progress in adsorptive membranes for separation—A review. *Sep. Purif. Technol.* **2020**, *255*, 117772. [CrossRef]
35. Isa, M.A.; Chew, T.L.; Yeong, Y.F. Zeolite NaY synthesis by using sodium silicate and colloidal silica as silica source. *IOP Conf. Ser. Mater. Sci. Eng.* **2018**, *458*, 012001. [CrossRef]

36. Lu, D.; Zou, H.; Guan, R.; Dai, H.; Lu, L. Sulfonation of polyethersulfone by chlorosulfonic acid. *Polym. Bull.* **2005**, *54*, 21–28. [CrossRef]
37. Kim, I.C.; Choi, J.G.; Tak, T.M. Sulfonated polyethersulfone by heterogeneous method and its membrane performances. *J. Appl. Polym. Sci.* **1999**, *74*, 2046–2055. [CrossRef]
38. Mthombo, T.S.; Mishra, A.K.; Mishra, S.B.; Mamba, B.B. The adsorption behavior of Cu(II), Pb(II), and Co(II) of ethylene vinyl acetate-clinoptilolite nanocomposites. *J. Appl. Polym. Sci.* **2011**, *121*, 3414–3424. [CrossRef]
39. Fei, F.; Cseri, L.; Szekely, G.; Blanford, C.F. Robust covalently cross-linked polybenzimidazole/graphene oxide membranes for high-flux organic solvent nanofiltration. *ACS Appl. Mater. Interfaces* **2018**, *10*, 16140–16147. [CrossRef]
40. Standardization Administration of the People's Republic of China. *HJ 486-2009*; Water Quality Determination of Copper 2, 9-Dimethy-1,10-Phenanthroline Spectrophotometric Method. Standards Press of China: Beijing, China, 2009.
41. Liu, Z.; Shi, C.; Wu, D.; He, S.; Ren, B. A simple method of preparation of high silica zeolite y and its performance in the catalytic cracking of cumene. *J. Nanotechnol.* **2016**, *2016*, 1486107. [CrossRef]
42. Zeng, Y.; Phadungbut, P.; Do, D.D.; Nicholson, D. Anatomy of adsorption in open-end and closed-end slit mesopores: Adsorption, desorption, and equilibrium branches of hysteresis loop. *J. Phys. Chem. C* **2014**, *118*, 25496–25504. [CrossRef]
43. Beck, J.S.; Vartuli, J.C.; Roth, W.J.; Leonowicz, M.E.; Kresge, C.T.; Schmitt, K.D.; Chu, C.T.W.; Olson, D.H.; Sheppard, E.W.; McCullen, S.B.; et al. A new family of mesoporous molecular sieves prepared with liquid crystal templates. *J. Am. Chem. Soc.* **1992**, *114*, 10834–10843. [CrossRef]
44. Kuleyin, A. Removal of phenol and 4-chlorophenol by surfactant-modified natural zeolite. *J. Hazard. Mater.* **2007**, *144*, 307–315. [CrossRef] [PubMed]
45. Chaudhry, S.A.; Zaidi, Z.; Siddiqui, S.I. Isotherm, kinetic and thermodynamics of arsenic adsorption onto Iron-Zirconium Binary Oxide-Coated Sand (IZBOCS): Modelling and process optimization. *J. Mol. Liq.* **2017**, *229*, 230–240. [CrossRef]
46. Li, X.; Xu, Q.; Han, G.; Zhu, W.; Chen, Z.; He, X.; Tian, X. Equilibrium and kinetic studies of copper(II) removal by three species of dead fungal biomasses. *J. Hazard. Mater.* **2009**, *165*, 469–474. [CrossRef]
47. Başar, C.A. Applicability of the various adsorption models of three dyes adsorption onto activated carbon prepared waste apricot. *J. Hazard. Mater.* **2006**, *135*, 232–241. [CrossRef]
48. Gok, O.; Ozcan, A.; Erdem, B. Prediction of the kinetics, equilibrium and thermodynamic parameters of adsorption of copper (II) ions onto 8-hydroxy quinoline immobilized bentonite. *Colloids Surf. A Physicochem. Eng. Asp.* **2008**, *317*, 174. [CrossRef]
49. Shen, J.; Li, K.; Muhammad, Y.; Zhang, N.; Guo, X.; Subhan, S.; Lan, C.; Liu, K.; Huang, F. Removal of Cu(II) ions from simulated wastewater using bagasse pith grafted polyacrylamide copolymer. *Chem. Eng. Res. Des.* **2020**, *164*, 361–372. [CrossRef]
50. Pooladi, A.; Bazargan-Lari, R. Simultaneous removal of copper and zinc ions by Chitosan/Hydroxyapatite/nano-Magnetite composite. *J. Mater. Res. Technol.* **2020**, *9*, 14841–14852. [CrossRef]
51. Kulkarni, P.; Watwe, V.; Pathak, G.; Sayyad, S.; Kulkarni, S. Evaluation of thermodynamic parameters via reaction stoichiometry and the corrected Langmuir parameter for sorption of Cu(II) on chitosan and chitosan blended PVA films. *J. Mol. Liq.* **2020**, *317*, 113962. [CrossRef]
52. Shi, W.; Zhang, F.; Zhang, G. Mathematical analysis of affinity membrane chromatography. *J. Chromatogr. A* **2005**, *1081*, 156–162. [CrossRef] [PubMed]
53. Pérez, P.; Aizman, A.; Contreras, R. Comparison between Experimental and Theoretical Scales of Electrophilicity Based on Reactivity Indexes. *J. Phys. Chem. A* **2002**, *106*, 3964–3966. [CrossRef]
54. Juang, R.-S.; Wu, F.-C.; Tseng, R.-L. Characterization and use of activated carbons prepared from bagasses for liquid-phase adsorption. *Colloids Surfaces A Physicochem. Eng. Asp.* **2002**, *201*, 191–199. [CrossRef]
55. Liu, P.; Wang, X.L.; Tian, L.; He, B.; Lv, X.; Li, X.; Wang, C.; Song, L. Adsorption of silver ion from the aqueous solution using apolyvinylidene fluoride functional membrane bearing thiourea groups. *J. Water Process Eng.* **2020**, *34*, 101184. [CrossRef]